

Article

# The Kinematic Analysis of a Wind Turbine Climbing Robot Mechanism

Jui-Hung Liu  and Kathleen Eborá Padrigalan \* 

Department of Mechanical Engineering, Southern Taiwan University of Science and Technology, No. 1, Nantai Street, Yung Kang District, Tainan City 710301, Taiwan; dofliu@stust.edu.tw

\* Correspondence: da81y202@stust.edu.tw; Tel.: +886-925-165-615

**Abstract:** The emergence of renewable energy offers opportunities for academia and the industry to conduct scientific research and innovative technological developments on wind turbine climbing robots. These robots were developed to carry out specialized application tasks, such as in-situ inspection and maintenance of wind turbine physical structure. This paper presents a scaled-down prototype design of a climbing robot for wind turbine maintenance and its kinematic modeling. The winding mechanism is the key feature for providing enough adhesion force to support the climbing robot and needs to adapt to the different diameters of the wind turbine tower, as it climbs through a circular truncated cone shape. A climbing model is then considered, using four mecanum wheels for maneuverability of the different movement states up-down, rotation, and spiral as it climbs the wind turbine tower. The design of the wind turbine climbing robot was modeled in SketchUp and the motion states were implemented in MATLAB for the climbing performance capabilities of the driving wheels of the robot. Based on the theoretical results of motion characteristics, the scaled-down prototype design of a climbing robot possesses maneuverability of motion and is able to predict the robot's performance. The contribution of this paper is intended to provide a basis for the new transformative climbing robot design and effectiveness of the mecanum wheel for robot motion.



**Citation:** Liu, J.-H.; Padrigalan, K.E. The Kinematic Analysis of a Wind Turbine Climbing Robot Mechanism. *Appl. Sci.* **2022**, *12*, 1210. <https://doi.org/10.3390/app12031210>

Academic Editors: Mihaiela Iliescu and Mingcong Deng

Received: 7 December 2021

Accepted: 21 January 2022

Published: 24 January 2022

**Publisher's Note:** MDPI stays neutral with regard to jurisdictional claims in published maps and institutional affiliations.



**Copyright:** © 2022 by the authors. Licensee MDPI, Basel, Switzerland. This article is an open access article distributed under the terms and conditions of the Creative Commons Attribution (CC BY) license (<https://creativecommons.org/licenses/by/4.0/>).

**Keywords:** climbing robot; maneuverability; mecanum wheel; kinematics

## 1. Introduction

The emergence of renewable energy is evident through the utilization of wind energy towards achieving a clean energy transformation. The world will become renewable-driven as new clean technology continues to be a core element of a strategy to revitalize the global economy. The demand change continues with an unprecedented shift that confronts some critical tasks to achieve wind turbine lifetime objectives while reducing the cost of inspections and maintenance because of various conditions such events of grease, hydraulic oil, flying planktons, extreme temperatures, wind speed variances, moistness, dust, radiation, lightning, saltiness and successive storms of rain, hail, snow, and sand [1]. Such events can create physical defects of the wind turbine that is difficult to detect in the early stage and can have a substantial effect on its performance efficiency over time. Detecting the wind turbine physical defects, corrosion, cracks, rust, loose bolts, material degradation, and faults are of great importance to improve the service life of wind turbines for long term operation [2,3]. Figure 1 shows the influence of various wind turbines' physical problems susceptible to environmental conditions and other factors.

The enormous wind energy growth offers opportunities for academe and industry to do scientific discipline, research innovation, and technological developments on wind turbine application robots to perform specific tasks. Such specific purpose and diverse application tasks are cleaning, painting, welding, repairing, material handling, object manipulation, inspection, diagnosis, and maintenance. The emergence of robots in wind turbine plays an important role in diverse applications that meets the need for demand and reduce maintenance cost.

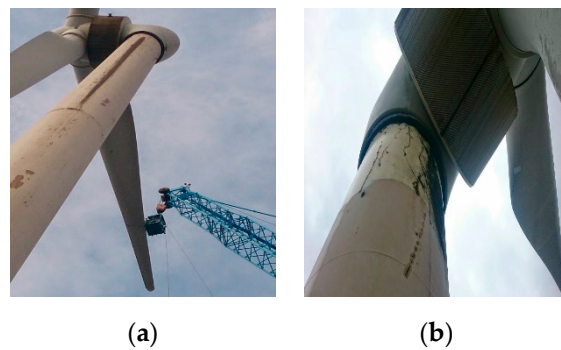


**Figure 1.** Wind turbine physical problems: (a) moistness and dust; (b) grease and hydraulic oil.

A climbing robot is a robotic system that is equipped with an appropriate locomotion and adhesion mechanism for adapting to the given environmental requirements [4]. A great number of studies have been devoted to wind turbine application with its various types of experimental prototypes and products have been proposed. For example, as shown in Table 1 the first model is the development of a “ring” climbing robot with a payload capability allowing it to climb around the cylindrical tower. The prototype has three modules that are completely identical and can be easily joined together to climb on any circumferential tube. The wheels depend on spring forces to grip around and climb on the tower. The innovation of the robot is that its adhesive forces are provided entirely by springs rather than conventional adhesion methods (such as vacuum suction, magnetic force, and dry adhesions) [5]; its drawback is that this type of locomotion needs an additional mechanism to turn the wheels at a certain angle to do the different movement states. The second model consists of a magnetic climbing robot for the inspection and maintenance of a wind power tower that utilizes four common kinds of strong magnetic units as one of the key components that adheres the robot to the tower. The robot is a track-based locomotion that has two modules connected with joints, and each module contains two tracks where steel segmented magnets are integrated. There are six magnetic units in one row-track that keep in contact with the tower surface as a plane [6]; its drawback is that this type of locomotion cannot directly change its own movement states. The third model is the two feet climbing robot on the rotor blade of the wind turbine. Its climbing technique is a modular approach that has two feet and three degrees of freedom, and each foot has three vacuum suckers installed in the vertex of the triangle to keep the robot in contact with the rotor blade. The robot can climb with a swing-around gait since the mechanical structure consists of a foot module and body module [7]; its drawback is that this type of locomotion does not easily execute various types of movement states due to its periodic gait patterns and adaptive gaits. The fourth model, the OmniClimber, has a high maneuverability for the inspection of ferromagnetic flat or convex structures, and it uses an omnidirectional magnetic wheel. The OmniClimber is new system development of its adaptable chassis, traction system, and central magnet. The central magnetic unit provides enough magnetic attraction force to hold the robot on the surface during robot action. The three-side magnets provide wheel traction to allow the robot to climb any structures without slippage [2]; its drawback is that this type of locomotion encounters noncontinuous contact due to the multiple adjustment system that causes a contactless interaction of the traction magnets to the wheel and surface structures. The fifth model is the Lego-based Robot, its bricks support the rapid transition towards the crawler, thus introducing continuous climbing instead of intermittent climbing. The robot utilizes tracks as locomotion and diagonal ropes were employed for the connection, while rubber bands contracted the system [8]; its drawback is that this type of locomotion is only limited to a single up-down movement. The sixth model, the Bladebug robot, uses suction to achieve adhesion to the blade. These six legs vacuum-padded feet robot perfectly adhere to blade surfaces and perform visual inspection [3]; the drawback of the six-leg design relates to a slowness of walking locomotion and its low payload capacity. The seventh

model, the magnetic climbing robot for the wind turbine tower, uses permanent magnets as an adhesion force. The robot uses four vertical wheels supported with eight shock absorbers to maintain the wheels in contact with the curvature of the tower. The robot can subsequently scan the blade surface to perform an inspection using various sensors to identify and classify damages [9]; its drawback is that this type of locomotion has a fixed orientation with a directed path in climbing up and down.

Table 1. Climbing robots used for wind turbine applications.

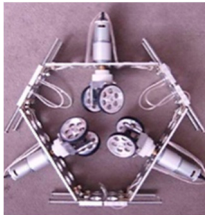
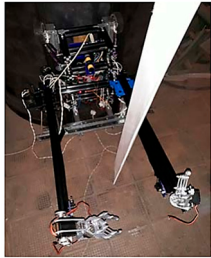
WT Climbing Robot	Image	Locomotion	Adhesion	Movement	Application Task
1 "Ring" Climb Robot [5]		Wheeled	Mechanical—spring traction	Up-Down Spiral Rotate	In-situ blade inspection
2 Magnetic Adhesion Robot [6]		Tracked	Magnetic	Up-Down Rotate	Inspection and maintenance of wind power tower
3 Two feet Climbing Robot [7]		Legged	Vacuum	Modular approach	Blade surface detection
4 OmniClimber Robot [2]		Omnidirectional Wheeled	Magnetic	Vertical Horizontal	Inspection and Maintenance
5 Lego-based Robot [8]		Tracked	Ropes/Rubber Bands traction	Up-Down	N/A

Table 1. Cont.

	WT Climbing Robot	Image	Locomotion	Adhesion	Movement	Application Task
6	BladeBug Robot [3]		Legged	Vacuum	N/A	Inspection and resurfacing the blades.
7	Magnetic Climbing Robot [9]		Wheeled	Magnetic	Up-Down	Blade inspection and tool handling

From the various wind turbine climbing robot studies, this research proposes a climbing robot that can move along on the wind turbine tower surface in different up-down movement states, and rotate and spiral using mecanum wheels to achieve its maximum maintenance efficiency where the robot needs to reach a pose on a specific tower area and perform in situ maintenance. The development of the mecanum wheel was pursued to further prove the effectiveness of this type of architecture and to add a transformative platform that is capable of remarkable maneuverability. Its multidirectional movements provide insights on the capability to move on circular truncated cone tower surfaces to document their performance addressing a vital industrial need of the rapid adoption of new clean technology. Through its exceptional maneuverability the robot can often deploy ancillary equipment to perform certain application tasks. The mecanum wheels are mounted in a fixed position and orientation with respect to the robot's body, provided that each wheel touches the tower surface as it travels. The wheel must touch around its point of contact on the tower to perform movement. The adhesion for the robot uses a winding mechanism, which uses a cable tension force to hold on the tower surface without falling to the ground, and to keep the robot in contact to the tower. This adhesion force needs to adapt the different diameter of the wind turbine tower, as it climbs through a circular truncated cone shape by winding and unwinding the cable through the help of the step motor.

Addressing the physical issues on the circular truncated cone shape of the wind turbine tower that are susceptible to environmental conditions, this paper proposed to design a climbing robot dedicated to this task or even to carry ancillary equipment to perform wind turbine maintenance. The robot can perform a tower surface visual inspection at any part of the tower structure as well as a wind turbine blades inspection, even in different weather conditions. The development of the robot has the payload capability of carrying inspection tools estimated to be at least 50% from the robot's total weight without breaking or slipping. Compared with previous studies, this proposed climbing robot utilizes a winding mechanism as an adhesion method and mecanum wheels as a locomotion method that takes advantage of maneuverability to do the different movement states up-down, rotation, and spiral to further prove the effectiveness of this robot design in performing maintenance of a wind turbine application. The comprehensive motion characteristics were defined through the kinematics analysis and innovative model to approximate the robot's position to optimize its climbing capability in a truncated cone tower.

In this paper, Section 2 gives the mechanical design of a scaled-down prototype of a wind turbine climbing robot and the robot's dimension in detail. Section 3 presents a kinematic analysis of a four mecanum wheel robot with a symmetrical structure and robot kinematic equation of motion that relates wheel velocity along the tower structure. To verify the correctness of the kinematic and motion, a theoretical analysis obtained from an estimated velocity were implemented through MATLAB in Section 4. Finally, conclusions and future work are described in Section 5.

## 2. Mechanical Design

### 2.1. Robot Design/Model

The structure of the climbing robot in a wind turbine tower is shown in Figure 2. The tower is a stand-alone steel tube with a varying diameter. The diameter varies between 330 mm at the tower top up to 400 mm at the tower bottom. The tower has a height of 1200 mm which has been adopted from a real 2 MW wind turbine which has a height of around 78,000 mm. The design of the wind turbine climbing robot consists of three parts: the driving mechanism, winding mechanism, and body frame is quite similar to what was demonstrated in [10] the first prototype. The second prototype addresses maneuverability and stability, resolving some of the issues that emerge in the first prototype.

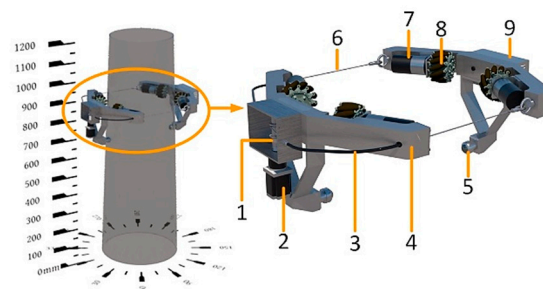


**Figure 2.** Wind Turbine Climbing Robot Model (1—Winding Mechanism with Twin Pulley, 2—Step Motor, 3—Bowden Cable, 4—Body Frame, 5—Caster Wheel, 6—Cable, 7—Motor, 8—Mecanum Wheel, 9—Electronic Casing-Embedded Microprocessor and Electronic module).

The driving mechanism are the four motorized mecanum wheels coated with rubber rollers around wheel circumference. It is adopted for obtaining maximum climbing speeds and includes different movement states: the up-down motion, rotational motion, and spiral motion. The maneuverability of the mecanum wheel possess three DOFs (degree of freedom) without slips due to its rubber-based roller. The first DOF is in the direction of the wheel orientation, and the second DOF is the motion of rollers mounted around the periphery of the main wheel. In principle, the roller axles can be mounted at any nonzero angle  $\varphi$  with respect to the wheel orientation. The mecanum wheel is shown in Figure 3, with roller axle angles of  $\varphi = \pm 45^\circ$  to the wheel axis. The third DOF is a rotational slip on the point of contact of the roller on the surface [11]. The construction of mecanum wheel rollers are left-handed wheels (rollers at  $-45^\circ$  to the wheel axis) and right-handed wheels (rollers at  $+45^\circ$  to the wheel axis). For left-handed mecanum wheels, rollers are orientated from lower right to upper left. Rollers for right-handed wheels are installed in the opposite way. The four motorized mecanum wheels will move along to a circular truncated cone tower with DC power supplies of 12 V. The CHP-36GP-BL3650 (Shenzhen Chihai Motor Co. Ltd., Shenzhen City, Guangdong, China) DC motors provide high torque and high power to drive the robot to its movement states. It is essential to emphasize that in the mecanum wheel, it is the wheel hub being controlled by a DC motor, but the wheel rollers are not. One of the key features of the climbing robot is the winding mechanism that utilizes a PL 36-37-42HS03 (Shenzhen Leadshine Control Technology Co. Ltd., Shenzhen City, Guangdong, China) step motor connected with a fabricated twin pulley and Bowden cable to provide the force to adhere the climbing robot on the tower surface. This mechanism will adjust to the different diameters of the circular truncated cone tower to grip on the

tower surface without falling to the ground. It maintains a safe distance through the help of a TOF10120 (Shenzhen Heng HongTong Electronics Technology Co. Ltd., Shenzhen City, Guangdong, China) laser range distance sensor that is attached to the robot's body frame. The distance sensor gives feedback signals to the embedded microprocessor module which is the Arduino MEGA 2560 (Shenzhen Ke Zhi You Technology Co. Ltd., Shenzhen City, Guangdong, China) that integrates all the controls of the movement states, winding mechanisms, and distance sensors. It will adjust depending on the tower diameter surface as it moves in different up-down motions, rotational motions, and spiral motions. With this design, the robot has the potential to adapt to the tapering wind turbine tower diameter structures and provides superior maneuverability capabilities to examine any physical problem of the tower, or taking specific application tasks. Once the climbing robot is set up on the tapered wind turbine tower, the frame is locked by the cable tension force as an adhesion mechanism of the robot. Lastly, the body frame is made of two parts to have a lightweight structure, ease of installation, and transport. The climbing robot possesses a caster wheel to increase the stability and support mechanism to its body frame to keep the mecanum wheels in contact with the tower. The embedded controller and other electronic accessories are attached to its body frame.

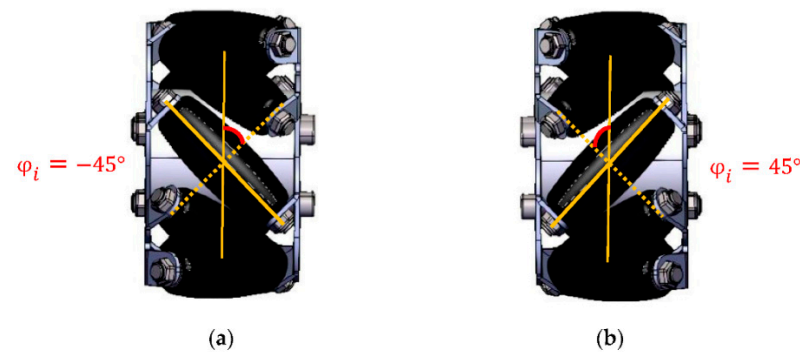


**Figure 3.** Mecanum wheel design: (a) Left mecanum wheel; (b) Right mecanum wheel.

## 2.2. Robot Dimension

The entire system of a climbing robot is made up of two body frames that have a winding mechanism, dimensions as reckoned with both top view and side view are shown in Figure 4.

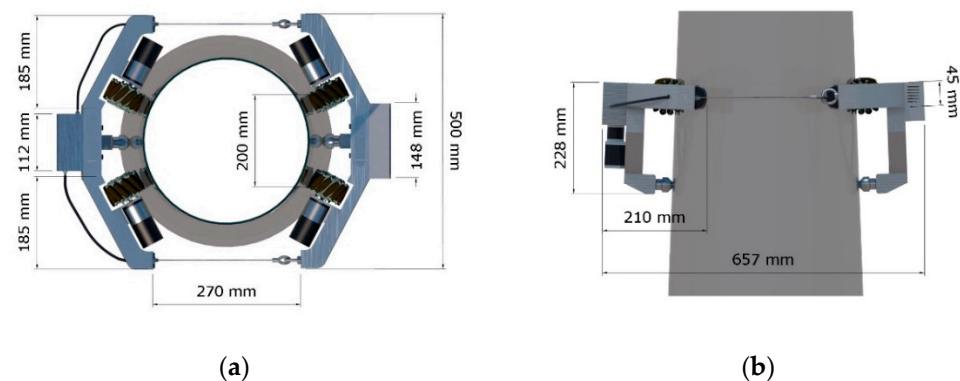


**Figure 4.** Climbing Robot Dimensions: (a) top view; (b) side view.

The robot has two body frames with a height of 45 mm, a length of 500 mm as shown in Figure 4, and the total robot weight of around 8 kg; it is made of aluminum alloy 6061 material which is lightweight and economical. The mecanum wheels have a diameter of 75 mm with 8 roller wheels. The roller wheels have a point of contact with the wind turbine tower which will constantly change as the robot moves along the tower surface. The tapering wind turbine tower is made of steel material with an average base diameter of

400 mm and the top diameter is of 330 mm. If the robot is at the lower segment of the tower, the diameter distance is increased, and as it moves upward, the diameter distance decreases. This change in diameter leads to a variation in length and forces. The winding adhesion provides the ideal traction force of the robot to move along the tower in different movement states: the up-down motion, rotational motion, and spiral motion. The mechanical design is carried out with the aid of SketchUp. The assumed velocity was carried out in MATLAB to calculate the speed of the mecanum wheels as the robot is in different movement states on a circular truncated cone tower, and holding onto the tower surface. The robot weight, wheel torque, traction force, and the coefficient of friction between the mecanum rubber roller wheel and tower surface were taken into consideration. The robot weight directly affects its ability to climb due to the gravitational force. Thus, this robot manifests a lightweight material that allows for a better efficiency of energy. The wheel torque must be at the equilibrium state where the robot moves with constant speed to attain the synchronization of body frame as it moves along the tower. The traction force must guarantee that the robot will adhere to the tower surface, ensuring that during the climbing process in the different movement states the robot will not fall. The coefficient of friction between the mecanum rubber roller wheel and metal tower surface are important to keep the robot moving safely where the wheels lock on the tower surface. Then, the robot’s weight, wheel torques, forces, and the inclination angle can be managed to meet the climbing scenario needed.

### 3. Kinematic Modeling

The entire structure of the scaled-down prototype climbing robot is composed of a body frame, mecanum wheels for locomotion, and a stepper motor coupled to a twin pulley and Bowden cable for adhesion. This structure facilitates kinematic modeling and focuses on the robot’s motion through the mecanum wheel movements. When the mecanum wheels are energized, the angled peripheral rollers translate a portion of the force in the rotational direction of the wheel to a force normal for the wheels’ direction. Depending on each individual wheel direction and velocity, the resulting combination of all these forces produce a total force vector in any desired direction. As a result, the robot can freely move in the direction of the corresponding force vector without the need to change the wheel orientation [12–16]. For a mecanum wheel to achieve multidirectional movements the wheels are arranged on the robot wheel configuration by mounting four wheels on the robot body frame on each side with a specified angle, as shown in Figure 5. To introduce this new transformative design of climbing robot, the position of the robot to the wind turbine tower and coordinate system needs to be defined.

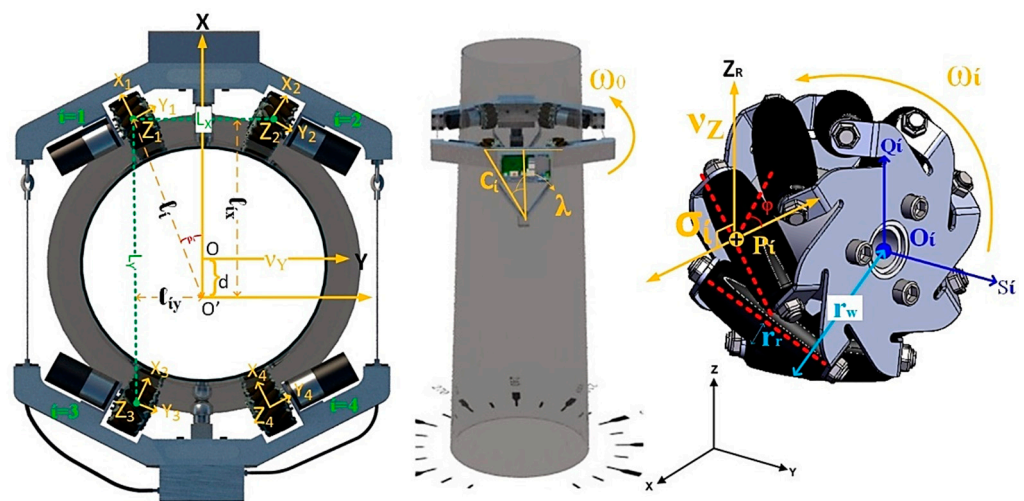


Figure 5. Coordinate System of WT Climbing Robot.

Let the radius of the mecanum wheel and roller be  $r_w$  and  $r_r$ , respectively; the angular velocity of four wheels to be  $\omega_1, \omega_2, \omega_3$  and  $\omega_4$  the speeds of rollers on each wheel to be  $v_{1r}, v_{2r}, v_{3r}$  and  $v_{4r}$  and the velocity of robot in Z-direction, Y-direction, and angular velocity in the X-axis around the center mass point  $O'$  to be  $v_Z, v_Y$  and  $\omega_0$ . The coordinate origins at  $O$ , the center of the robot, and each wheel have an origin of  $O_1, O_2, O_3$  and  $O_4$ . The distance between the wheel 1 and 2 center point of the robot wheels is while the distance between the wheel 1 and 3 center point of robot wheels is  $L_Y$ , the wheels' axis of rolling  $\varphi_i$  is the angle of the rollers which is  $\pm 45^\circ$ , in this case shown in Figure 3, the layout of the rollers. The  $\sigma_i$  is the angle between  $P_i$  to  $Z_R$ . The  $C_i$  is the distance from the center point of the caster wheel to the center point of the robot wheels. The  $\lambda$  is the angle between  $C_i$  and the distance from the center of the body frame to the center point of the caster wheel. The  $v_{S_i}$  and  $v_{Q_i}$  represent the velocity of the wheel  $i$  in the  $S_i O_i Q_i$  coordinate system.

According to Figure 5 the velocity of the wheel  $i$  and the layout of the rollers in contact to the mockup wind turbine tower without slipping can be derived by:

$$v_{S_i} = v_{ir}(\sin \varphi) \tag{1}$$

$$v_{Q_i} = \omega_i (r_i) - v_{ir}(\cos \varphi) \tag{2}$$

The velocity of the wheel's center translated to the robot can be expressed  $Z_R O' Y_R$  as a coordinate system can be achieved by the Equations (3) and (4).

$$v_{iZ_R} = v_Z + (C_i \sin \lambda) \omega_0 \tag{3}$$

$$v_{iY_R} = v_Y + (C_i \cos \lambda) \omega_0 \tag{4}$$

The moving velocity of the wheel  $i$  in the robot coordinate system can be obtained from the Equations (5) and (6).

$$v_{ir}(\sin \varphi) = v_Y + (C_i \cos \lambda) \omega_0 \tag{5}$$

$$\omega_i (r_i) - v_{ir}(\cos \varphi) = v_Z + (C_i \sin \lambda) \omega_0 \tag{6}$$

From Equations (5) and (6), Equation (7) can derive the velocity of the roller in the  $i$ th wheel and Equation (9) the wheels' angular velocity:

$$v_{ir} = \frac{v_Y + (C_i \cos \lambda) \omega_0}{\sin \lambda} \tag{7}$$

$$\omega_i(r_i) = v_Z + \omega_0(C_i \sin \lambda) + (v_Y + \omega_0(C_i \cos \lambda)) \left( \frac{\cos \varphi}{\sin \varphi} \right) \tag{8}$$

$$\omega_i = \frac{1}{r} \left[ 1 \quad \frac{\cos \varphi}{\sin \varphi} \quad C_i \sin \lambda + (C_i \cos \lambda) \left( \frac{\cos \varphi}{\sin \varphi} \right) \right] \begin{bmatrix} v_Z \\ v_Y \\ \omega_0 \end{bmatrix} \tag{9}$$

Since there is a relationship between the independent variable  $v_{ir}$  and  $\omega_i$  in each joint, angular and linear velocities, assuming there is no slip on the tower surface, the changes in the magnitude and direction of angular velocity of four wheels  $\omega_1, \omega_2, \omega_3$  and  $\omega_4$  can affect the speeds of rollers on each wheel to be  $v_{1r}, v_{2r}, v_{3r}$  and  $v_{4r}$  which consequently achieve the movement of the robot.

$$\begin{bmatrix} \omega_1 \\ \omega_2 \\ \omega_3 \\ \omega_4 \end{bmatrix} = \frac{1}{r} \begin{bmatrix} 1 & \frac{1}{\tan \varphi} & -\left(C_i \sin \lambda + \frac{C_i \cos \lambda}{\tan \varphi}\right) \\ 1 & \frac{-1}{\tan \varphi} & \left(C_i \sin \lambda + \frac{C_i \cos \lambda}{\tan \varphi}\right) \\ 1 & \frac{-1}{\tan \varphi} & -\left(C_i \sin \lambda + \frac{C_i \cos \lambda}{\tan \varphi}\right) \\ 1 & \frac{1}{\tan \varphi} & \left(C_i \sin \lambda + \frac{C_i \cos \lambda}{\tan \varphi}\right) \end{bmatrix} \begin{bmatrix} v_Z \\ v_Y \\ \omega_0 \end{bmatrix} \tag{10}$$

Considering the facts that wheels have the same size, the offset angle of the roller  $\varphi = 45^\circ$ , the transformation matrix is:

$$\begin{bmatrix} \omega_1 \\ \omega_2 \\ \omega_3 \\ \omega_4 \end{bmatrix} = \frac{1}{r} \begin{bmatrix} 1 & 1 & -\left(C_i \sin \lambda + \frac{C_i \cos \lambda}{\tan \varphi}\right) \\ 1 & -1 & \left(C_i \sin \lambda + \frac{C_i \cos \lambda}{\tan \varphi}\right) \\ 1 & -1 & -\left(C_i \sin \lambda + \frac{C_i \cos \lambda}{\tan \varphi}\right) \\ 1 & 1 & \left(C_i \sin \lambda + \frac{C_i \cos \lambda}{\tan \varphi}\right) \end{bmatrix} \begin{bmatrix} v_Z \\ v_Y \\ \omega_o \end{bmatrix} \tag{11}$$

By replacing the parameters of matrix Equation (11), let  $E = C_i \sin \lambda$  and  $F = C_i \cos \lambda$  will be Equation (12).

$$\begin{bmatrix} \omega_1 \\ \omega_2 \\ \omega_3 \\ \omega_4 \end{bmatrix} = \frac{1}{r} \begin{bmatrix} 1 & 1 & -(E + F) \\ 1 & -1 & (E + F) \\ 1 & -1 & -(E + F) \\ 1 & 1 & (E + F) \end{bmatrix} \begin{bmatrix} v_Z \\ v_Y \\ \omega_o \end{bmatrix} \tag{12}$$

The inverse kinematic solves the individual wheel speed that the velocity of the system can be obtained by implementing  $\omega_i$ , the wheel angular velocity and  $v_{ir}$ , the velocity of passive rollers in the wheel  $i$  can be achieved by Equation (13) and its corresponding matrix from Equation (11).

$$\begin{bmatrix} \omega_i \\ v_{ir} \end{bmatrix} = T \begin{bmatrix} v_Z \\ v_Y \\ \omega_o \end{bmatrix} \tag{13}$$

In contrary, the equation specifying the velocities is the forward kinematic according to Equations (14) and (15).

$$\begin{bmatrix} v_Z \\ v_Y \\ \omega_o \end{bmatrix} = T^+ \begin{bmatrix} \omega_i \\ v_{ir} \end{bmatrix} \tag{14}$$

$$\begin{bmatrix} v_Z \\ v_Y \\ \omega_o \end{bmatrix} = T^+ \begin{bmatrix} \omega_1 \\ \omega_2 \\ \omega_3 \\ \omega_4 \end{bmatrix} \tag{15}$$

$T$  is the transformation matrix of the inverse equation of motion that corresponds to Equation (11).

$$T = \frac{1}{r} \begin{bmatrix} 1 & 1 & -\left(C_i \sin \lambda + \frac{C_i \cos \lambda}{\tan \varphi}\right) \\ 1 & -1 & \left(C_i \sin \lambda + \frac{C_i \cos \lambda}{\tan \varphi}\right) \\ 1 & -1 & -\left(C_i \sin \lambda + \frac{C_i \cos \lambda}{\tan \varphi}\right) \\ 1 & 1 & \left(C_i \sin \lambda + \frac{C_i \cos \lambda}{\tan \varphi}\right) \end{bmatrix} \tag{16}$$

The expression of its pseudoinverse matrix  $T^+$  is generalized by:

$$T^+ = (T^T T)^{-1} T^T \tag{17}$$

$$T^+ = \frac{r}{4} \begin{bmatrix} 1 & 1 & 1 & 1 \\ 1 & -1 & -1 & 1 \\ -(E + F) & (E + F) & -(E + F) & (E + F) \end{bmatrix} \tag{18}$$

In this model the forward kinematic equation of the system is obtained:

$$\begin{bmatrix} v_Z \\ v_Y \\ \omega_o \end{bmatrix} = \frac{r}{4} \begin{bmatrix} 1 & 1 & 1 & 1 \\ 1 & -1 & -1 & 1 \\ -(E + F) & (E + F) & -(E + F) & (E + F) \end{bmatrix} \begin{bmatrix} \omega_1 \\ \omega_2 \\ \omega_3 \\ \omega_4 \end{bmatrix} \quad (19)$$

For the up-down motion the Z-axis velocity is not zero, while the Y-axis and the angular velocity are zero, then Equation (18) is obtained.

$$v_Z(t) = \frac{r}{4} (\omega_1 + \omega_2 + \omega_3 + \omega_4) \quad (20)$$

For the rotational motion the Y-axis is not zero, while the Z-axis and angular velocity are zero, then Equation (19) is obtained.

$$v_Y(t) = \frac{r}{4} (\omega_1 - \omega_2 - \omega_3 + \omega_4) \quad (21)$$

For the spiral motion both Z-axis and Y-axis is not zero, while angular velocity is zero it can be concluded that:

$$v_{ZY}(t) = \frac{r}{4} (\omega_1 + \omega_2 + \omega_3 + \omega_4) + \frac{r}{4} (\omega_1 - \omega_2 - \omega_3 + \omega_4) \quad (22)$$

$$v_{ZY}(t) = \frac{r}{2} (\omega_1 + \omega_4) \quad (23)$$

Then the angular velocity is not zero, Equation (20) can be obtained:

$$\omega_o(t) = \frac{r}{4} [-(E + F)\omega_1 + (E + F)\omega_2 - (E + F)\omega_3 + (E + F)\omega_4] \quad (24)$$

The Equations (18)–(20) show the relationship between the angular velocity of the wheels and the movement of the robot in its different movement states. The presence of the four added DC motors is considered an essential kinematic equation of motion because an equation that relates velocity has a direct control of the wheel velocity. The robot parameters as shown in Table 2 with the wheels are mounted in a fixed angle position and orientation with respect to the robot body frame provided that each wheel touches the wind turbine tower surface as it travels.

**Table 2.** Climbing Robot Parameters.

$i$	Wheels	$\sigma_i$	$\varphi_i$	$\lambda$
1	1	90°	45°	24.44°
2	2	90°	−45°	24.44°
3	3	90°	−45°	24.44°
4	4	90°	45°	24.44°

The simulation of the robot’s projected movements was implemented in MATLAB. The rotational speeds of the wheels were calculated using the climbing robot parameters and the kinematic equations. Since there are three movement states (up-down, rotation, and spiral), the distance traveled by the robot during these states are also calculated. For the up-down movement, the distance used was the tower’s height, which is 1200 mm. For the rotation of the robot at a point in the tower, the circumference is used, which is 1184 mm. This is taken at a point on the tower where the diameter is 400 mm. Then for the spiral movement, the length of the spiral was calculated using an Archimedean spiral

along a circular truncated cone. The formula is presented in Equation (25), reaching a value of 8885 mm.

$$\int_a^b \sqrt{r^2 + \left(\frac{dr}{d\theta}\right)^2} d\theta \quad (25)$$

The velocities  $v_Z$  and  $v_Y$  were assumed, such that they reflect the ideal movement scenarios for our robot. For instance, if the robot climbs up the tower at a constant speed,  $v_Z$  is an arbitrary positive value, while  $v_Y$  is zero since it is not rotating around the tower. On the other hand, if the robot goes down the tower,  $v_Z$  is an arbitrary negative value, while  $v_Y$  is zero. For the rotation of the robot around the tower,  $v_Y$  is a positive value if it is rotating to the right and  $v_Z$  is zero, as the robot is not moving up or down the tower. If the robot is to rotate to the left,  $v_Y$  is a negative value if it is rotating to the right and  $v_Z$  is zero. For spiral movements, velocities  $v_Z$  and  $v_Y$  have nonzero values. Positive values indicate upward movement for  $v_Z$ , while for  $v_Y$ , it indicates rotation to the right. Negative values indicate downward movement for  $v_Z$ , while for  $v_Y$ , it indicates rotation to the left. For instance, if the robot is moving spiral-left-upward,  $v_Z$  is positive and  $v_Y$  is negative. If it is moving-spiral left-downward,  $v_Z$  and  $v_Y$  are negative. If the robot is moving spiral-right-upward,  $v_Z$  and  $v_Y$  are positive. If it is moving spiral-right-downward,  $v_Z$  is negative and  $v_Y$  is positive. The  $\omega_0$  was set to 0 as it is the rotation of the robot at the X-axis. This is not an ideal scenario for the movement of the robot, as it should only rotate at the Z-axis.

#### 4. Results and Discussion

The study of the motion of the climbing robot travelling on the surface of the tower was tested through the MATLAB environment, which showed reasonable motion of the robot. The assumed velocities were to demonstrate full functionality of the kinematic modeling for the robot, where the results presented are very satisfactory. Theoretically, the robot can move in the specified movement states without changing its orientation by a proper combination of the four wheels' angular velocity. In fact, for this climbing robot, the commonly used movements are being studied to evaluate the effectiveness of the mecamum wheel as locomotion. Figure 6 shows the climbing robot wheel movement in different states. Moving all four wheels inwardly and outwardly causes an up-down movement of the robot on the tower, running the two wheels on one side in an opposite direction either inwardly or outwardly to those on the other side, which causes rotational movement to the tower and running one wheel on one side either inwardly or outwardly to those on the other side, which causes spiral movement. The robot has been designed in such a way that the wheels of the right or left side could be exchanged between them. The eight movement states are attained by adopting the wheel combination technique.

The assumed velocity is 120 mm/s as it is provided in Table 3, to ensure a promising result with respect to climbing performance capability in a certain motion, particularly speed and stability. It is also assumed that there is no wheel slip on the tower as it climbs. The climbing modeled along the desired path as it moves to the wind turbine tower are shown in Figure 7. The motion of the robot along the tower allows examining the path as it goes in an up-down motion, rotation from left-right motion, spiral left-right, and upward-downward motion as shown in Figure 7a–d. The climbing model of the robot motions along the wind turbine tower with the height of 1200 mm and 330–400 mm tower diameter. The movement states of the robot are along the Z, Y and X axes. The angular speed for each wheel is assumed to be 3 rad/s, which is multiplied by each wheel's velocity both in up-down and rotational movements. For the spiral motion, the calculated distance travelled was based on the length of an Archimedean spiral. Thus, the total distance travelled by the robot is 8885 mm. To achieve the spiral movement the velocities of the two wheels are 5 rad/s each, and the other two wheels are zero. Travelling along the defined path provides the current pose of the robot. It is considered that a mecamum wheel has good stability in the motion process with enough adhesion to grip on the tower surface.

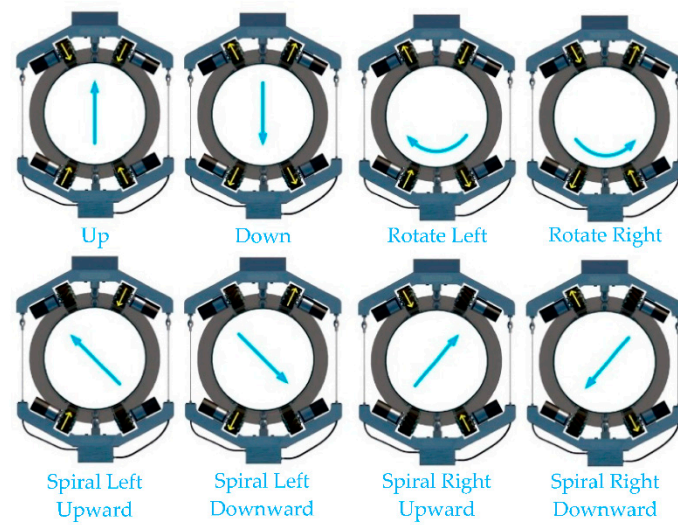


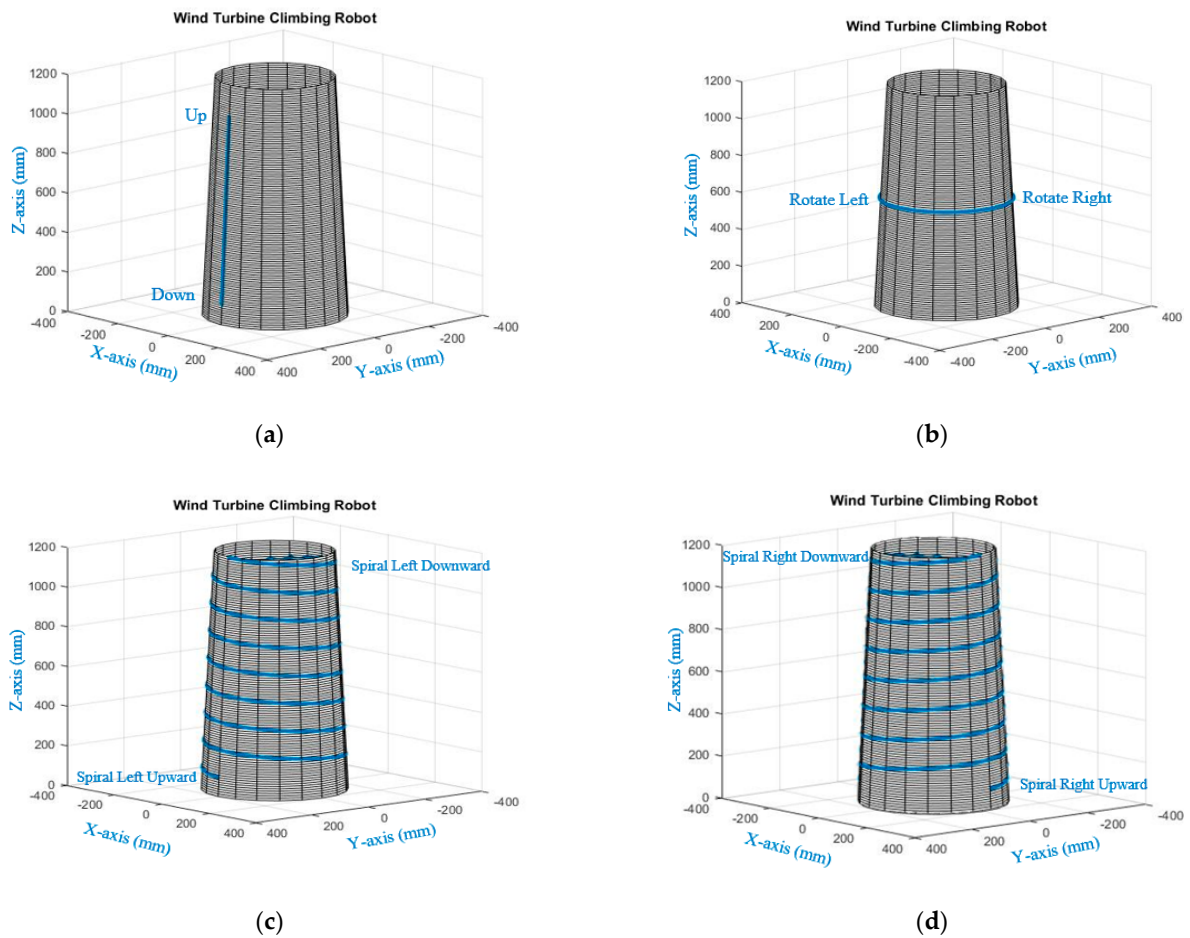
Figure 6. Climbing robot wheel movement states.

Table 3. Assumed Velocities and Results.

Direction	$v_z$	$v_y$	$\omega_0$	Wheel 1	Wheel 2	Wheel 3	Wheel 4
Up	120 mm/s	0	0	3 rad/s	3 rad/s	3 rad/s	3 rad/s
Down	-120 mm/s	0	0	-3 rad/s	-3 rad/s	-3 rad/s	-3 rad/s
Rotate Left	0	-120 mm/s	0	-3 rad/s	3 rad/s	3 rad/s	-3 rad/s
Rotate Right	0	120 mm/s	0	3 rad/s	-3 rad/s	-3 rad/s	3 rad/s
Spiral Left Upward	120 mm/s	-120 mm/s	0	0 rad/s	5 rad/s	5 rad/s	0 rad/s
Spiral Left Downward	-120 mm/s	-120 mm/s	0	0 rad/s	-5 rad/s	-5 rad/s	0 rad/s
Spiral Right Upward	120 mm/s	120 mm/s	0	5 rad/s	0 rad/s	0 rad/s	5 rad/s
Spiral Right Downward	-120 mm/s	120 mm/s	0	-5 rad/s	0 rad/s	0 rad/s	-5 rad/s

The robot’s ideal motion as shown in Figure 8 with robot velocity and total distance traveled. Figure 8a shows the up-down motion that the robot velocity is expected to increase from 0 mm/s to reach the maximum value of 120 mm/s as a commendable range with the corresponding tower distance that is within 0–1200 mm. Figure 8b shows the rotate motion that the robot velocity is expected to increase from 0 mm/s to reach the maximum value of 120 mm/s as a commendable range with the corresponding tower circumference within 0–1184 mm. Figure 8c shows the spiral motion the robot velocity is expected to increase from 0 mm/s to reach the maximum value of 170 mm/s as a commendable range with the corresponding ZY-axis from a total distance of 0–8885 mm.

Table 3 also shows the 8 corresponding wheel directions up, down, rotate left, rotate right, spiral-left-upward, spiral-left-downward, spiral-right-upward and spiral-right-downward. For the up direction all four wheels are positioned inwardly to the tower surface and for down direction all four wheels are positioned outwardly to the tower surface. For the rotation to the left, the wheels 1 and 4 are facing outward while the wheels 2 and 3 are inward to the tower surface. For the rotation to the right, the wheels 1 and 4 are inward while the wheels 2 and 3 are outward to the tower surface. For the spiral to the left upward, the wheels 2 and 3 are inward to the tower surface while the spiral to the left downward the wheels 2 and 3 are outward to the tower surface. For the spiral to the right upward, the wheels 1 and 4 are inward to the tower surface while the spiral to the right downward the wheels 1 and 4 are outward to the tower surface. We consider that all mecanum wheels will spin on the estimated rotational speed to achieve all the driving directions.



**Figure 7.** Climbing modeled along the desired path: (a) up-down motion; (b) rotation from left-right; (c) spiral left and upward-downward; (d) spiral right and upward-downward.

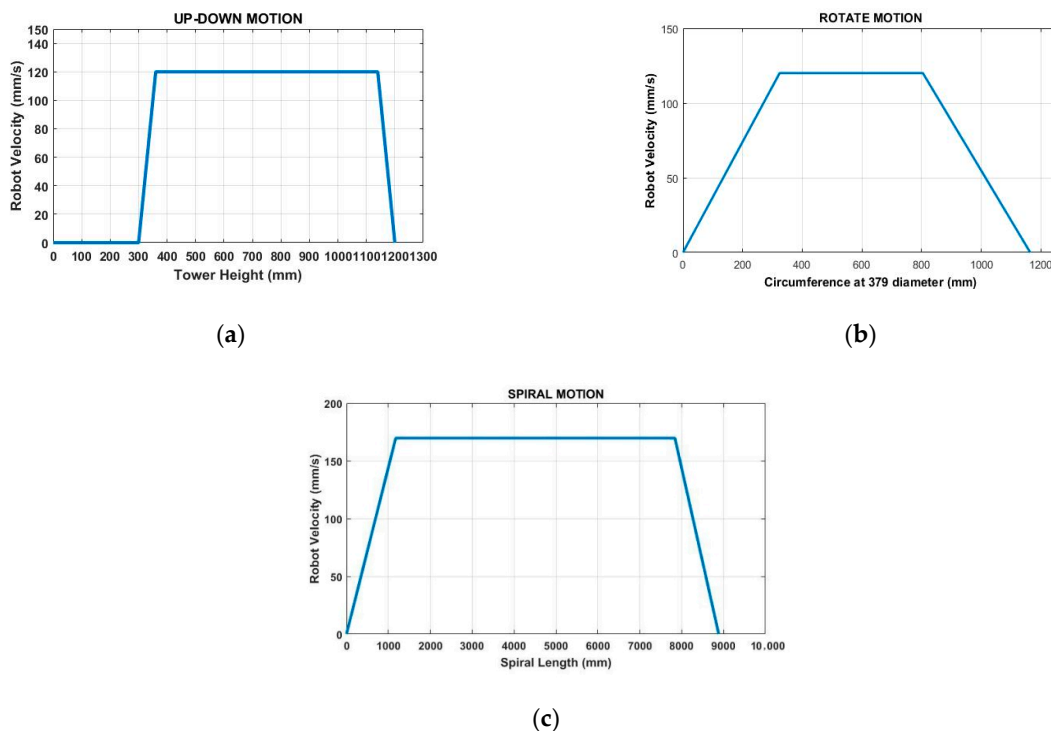


**Figure 8.** Robot Ideal Motion: (a) up-down; (b) rotation; (c) spiral.

## 5. Conclusions and Future Work

In this paper, the scaled-down prototype design of a climbing robot for wind turbine was presented with a kinematic analysis on its different movement states. The results show that the robot can perform the eight movement states including up-down, rotation from left-right, spiral left upward-downward, and spiral right upward-downward. The kinematic equations were implemented through MATLAB, using matrix analysis. The resulting wheel speeds of the robot to move along the tower surface showed a reasonable velocity based on mathematical equations and an initial prototype. Theoretical results showed that mecanum wheels in the robot can achieve the specified movement states along the tower surface without changing its orientation. The calculated mecanum wheel speeds obtained from the MATLAB using the derived kinematic equations prove to predict the climbing performance of the wind turbine climbing robot and evaluate its design rationality and effectivity. Moreover, this paper shares a new transformative design of a climbing robot for wind turbine capable of agile using the mecanum wheels as its locomotion and a cable tension force as its adhesion. Future work includes the implementation of the actual prototype testing as the basis for the effectiveness of the mecanum wheel for the robot's motion and design.

**Author Contributions:** Conceptualization: J.-H.L.; data collection: K.E.P.; theoretical analysis: J.-H.L. and K.E.P.; experiment and test: J.-H.L. and K.E.P.; writing-original draft: J.-H.L. and K.E.P.; writing-review and editing: J.-H.L. and K.E.P. All authors have read and agreed to the published version of the manuscript.

**Funding:** This research received no specific grant from any funding agency.

**Institutional Review Board Statement:** Not applicable.

**Informed Consent Statement:** Not applicable.

**Data Availability Statement:** Data sharing not applicable.

**Conflicts of Interest:** The authors declare no conflict of interest.

## References

1. Kumar, A.; Khan, M.Z.U.; Pandey, B.; Mekhilef, S. Wind Energy: A Review Paper. *Gyancity J. Eng. Technol.* **2018**, *4*, 29–37. [[CrossRef](#)]
2. Tavakoli, M.; Viegas, C.; Marques, L.; Pires, J.N.; de Almeida, A.T. OmniClimbers: Omni-directional magnetic wheeled climbing robots for inspection of ferromagnetic structures. *Robot. Auton. Syst.* **2013**, *61*, 997–1007. [[CrossRef](#)]
3. Bogue, R. Climbing robots: Recent research and emerging applications. *Ind. Robot.* **2019**, *46*, 721–727. [[CrossRef](#)]
4. Chu, B.; Jung, K.; Han, C.-S.; Hong, D. A survey of climbing robots: Locomotion and adhesion. *Int. J. Precis. Eng. Manuf.* **2010**, *11*, 633–647. [[CrossRef](#)]
5. Sattar, T.P.; Rodriguez, H.L.; Bridge, B. Climbing ring robot for inspection of offshore wind turbines. *Ind. Robot.* **2009**, *36*, 326–330. [[CrossRef](#)]
6. Gao, X.; Shao, J.; Dai, F.; Zong, C.; Guo, W.; Bai, Y. Strong Magnetic Units for a Wind Power Tower Inspection and Maintenance Robot. *Int. J. Adv. Robot. Syst.* **2012**, *9*, 189. [[CrossRef](#)]
7. Wang, B.; Luo, H.; Jin, Y.; He, M. Path Planning for Detection Robot Climbing on Rotor Blade Surfaces of Wind Turbine Based on Neural Network. *Adv. Mech. Eng.* **2013**, *5*, 760126. [[CrossRef](#)]
8. Franko, J.; Du, S.; Kallweit, S.; Duelberg, E.; Engemann, H. Design of a Multi-Robot System for Wind Turbine Maintenance. *Energies* **2020**, *13*, 2552. [[CrossRef](#)]
9. Sahbel, A.; Abbas, A.; Sattar, T. System Design and Implementation of Wall Climbing Robot for Wind Turbine Blade Inspection. In Proceedings of the 2019 International Conference on Innovative Trends in Computer Engineering (ITCE), Aswan, Egypt, 19 February 2019; pp. 242–247. [[CrossRef](#)]
10. Liu, J.-H.; Padrigalan, K. Design and Development of a Climbing Robot for Wind Turbine Maintenance. *Appl. Sci.* **2021**, *11*, 2328. [[CrossRef](#)]
11. Muir, P.F.; Neuman, C.P. Kinematic modeling of wheeled mobile robots. *J. Robot. Syst.* **1987**, *4*, 281–340. [[CrossRef](#)]
12. Zhang, Y.; Ge, S. Analysis of the motion characteristics of Marine Mecanum transport platform. *MATEC Web Conf.* **2018**, *232*, 04006. [[CrossRef](#)]
13. Rojas, R.; Forster, A.G. Holonomic Control of a robot with an omni-directional drive. *KI-Kunstl. Intell.* **2006**, *20*, 12–17.
14. Taheri, H.; Qiao, B.; Ghaeminezhad, N. Kinematic Model of a Four Mecanum Wheeled Mobile Robot. *Int. J. Comput. Appl.* **2015**, *113*, 6–9. [[CrossRef](#)]

15. Li, Y.; Ge, S.; Dai, S.; Zhao, L.; Yan, X.; Zheng, Y.; Shi, Y. Kinematic Modeling of a Combined System of Multiple Mecanum-Wheeled Robots with Velocity Compensation. *Sensors* **2019**, *20*, 75. [[CrossRef](#)] [[PubMed](#)]
16. Yamada, N.; Komura, H.; Endo, G.; Nabae, H.; Suzumori, K. Spiral Mecanum Wheel achieving omnidirectional locomotion in step-climbing. In Proceedings of the 2017 IEEE International Conference on Advanced Intelligent Mechatronics (AIM), Munich, Germany, 3 July 2017; pp. 1285–1290. [[CrossRef](#)]